frontiers | Frontiers in Earth Science

ORIGINAL RESEARCH
published: 12 July 2022
doi: 10.3389/feart.2022.927159

Experimental Study on Damage Properties of Granites Under Flowing Acid Solution

Wei Chen[1,2], Wen Wan[2], Yanlin Zhao[2], Qiuhong Wu[2], Huan He[3], Wenqing Peng[2], Xiaofan Wu[4], Yu Zhou[2], Li Wu[5] and Senlin Xie[6]*

[1]Department of Building Engineering, Hunan Institute of Engineering, Xiangtan, China, [2]School of Resource, Environment and Safety Engineering, Hunan University of Science and Technology, Xiangtan, China, [3]Mianyang Economic-Technological Development Zone, Sichuan University of Culture and Arts, Mianyang, China, [4]School of Mathematics and Computational Science, Hunan University of Science and Technology, Xiangtan, China, [5]School of Earth Sciences and Spatial Information Engineering, Hunan University of Science and Technology, Xiangtan, China, [6]School of Energy and Mining Engineering, China University of Mining and Technology (Beijing), Beijing, China

In order to study the deterioration characteristics of the tunnel surrounding rock under the scouring of flowing groundwater, we ratioed similar acidic solutions based on groundwater composition. The microstructure of granite samples cored on site, deformation features, and evolution characteristics of mechanical parameters under saturations with different flow rates and various pH values were analyzed using scanning electron microscopy (SEM), energy dispersive spectroscopy (EDS), nuclear magnetic resonance (NMR), and X-ray diffraction (XRD). The results indicate the following: 1) compared with the static water condition, the higher flow rate produces greater relative changes in granite's microstructure, porosity, mass, and pH of the immersed solution. Moreover, the rate of change is relatively fast in the early stage and gradually slows down until it reaches a stable state. 2) Compared with the natural dry condition, the solution with a lower pH value causes the structural framework of the specimen to loosen, the mass loss degree to increase, and the porosity dispersion to intensify. 3) The dynamic water is more sensitive than the static water to the elastic vertical wave velocity of granite. Compared with the dry sample, the elastic longitudinal wave velocity of the sample in acidic solution with pH = 2 and flow rates of 0, 150, and 300 mm·s^{-1} for 49 days decreased by 8.7, 10.9, and 13.5%, respectively, which accelerates the instability and failure of the granite surroundings.

Keywords: granite surroundings, rock mechanics parameters, effect of solution velocity, hydration corrosion, damage mechanism

OPEN ACCESS

Edited by:
Thomas Hermans,
Ghent University, Belgium

Reviewed by:
Bing Bai,
Beijing Jiaotong University, China
Xiangxin Liu,
North China University of Science and Technology, China

****Correspondence:***
Wei Chen
chenweiwade@mail.hnust.edu.cn

Specialty section:
This article was submitted to Structural Geology and Tectonics, a section of the journal Frontiers in Earth Science

Received: *23 April 2022*
Accepted: *30 May 2022*
Published: *12 July 2022*

Citation:
Chen W, Wan W, Zhao Y, Wu Q, He H, Peng W, Wu X, Zhou Y, Wu L and Xie S (2022) Experimental Study on Damage Properties of Granites Under Flowing Acid Solution. Front. Earth Sci. 10:927159. doi: 10.3389/feart.2022.927159

1 INTRODUCTION

The surrounding rock in underground engineering has been longtime damaged and degraded by various physical and chemical actions (Dong et al., 2020; Liu et al., 2020; Bai et al., 2021; Zhao et al., 2021b). For instance, during groundwater flow, the rock mass will not only happen to softening, migration, argillization, and other physical effects but produce the chemical reaction such as ion exchange, dissolution, and hydrolysis, which will bring about the changes in overall structure, mineral composition, and physical properties of surrounding rock and will accordingly deteriorate its mechanical properties to cause engineering accidents (Bai et al., 2017; Liu et al., 2019; Zhao et al., 2021b).

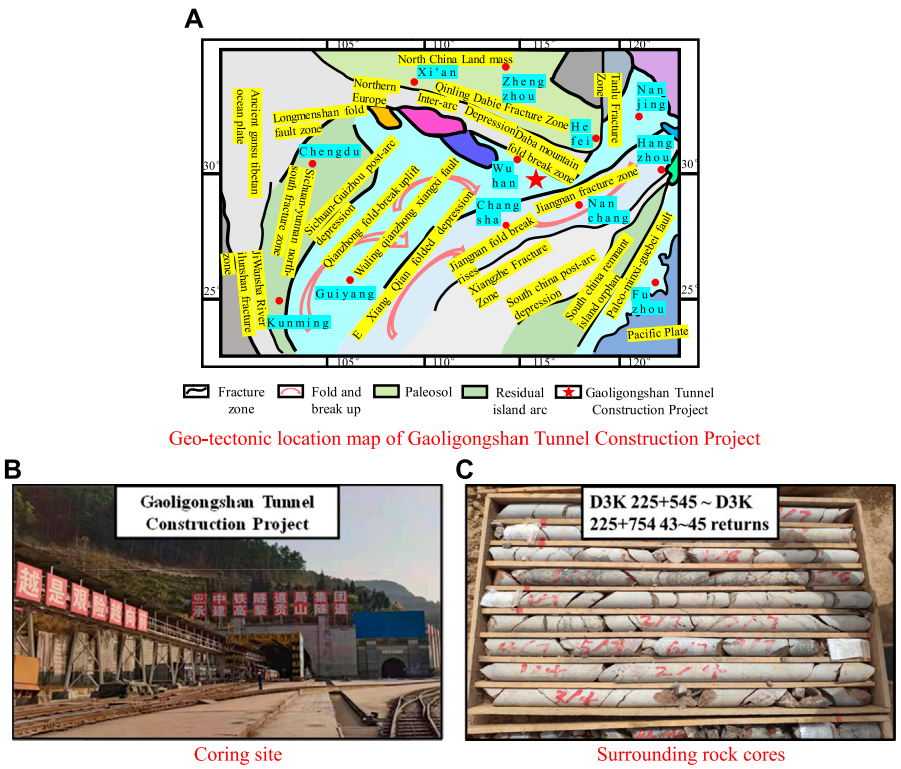

FIGURE 1 | Preparation process of granite specimens. **(A)** Geo-tectonic location map of Gaoligongshan Tunnel Construction Project. **(B)** Coring site. **(C)** Surrounding rock cores.

Currently, rich achievements have been made for the different aqueous chemical solutions to the macro–microstructure of rocks and physical and mechanical properties of damage effects. Huang et al. (2021) studied the changes in chroma, mass, vertical wave velocity, porosity, thermal conductivity, and tensile strength of granite, sandstone, and marble induced by chemical erosion and found that rock materials exhibit varying degrees of changes in physical and mechanical properties under the action of acidic solution corrosion. Huo et al. (2018) and Li et al. (2021) discussed the physical-chemical properties and mechanical properties of sandstone after saturations in different acid solutions and established the dynamical model of acid rock reaction. Through triaxial rheological tests, Xie et al. (2011) found out that chemical corrosion greatly accelerated the instantaneous strain rate of limestone under triaxial stress. Chen et al. (2021) derived the damage evolution equation and constitutive model of acid-corroded rock under the coupling effect of freezing–thawing and confining pressure based on the theory of continuous damage mechanics and carried out triaxial compression test to further reveal the damage mechanism and failure law of acid-corroded rock under the coupling effect of freezing–thawing and confining pressure. Wang et al. (2021) soaked the granite in nitric acid with different pH values and analyzed the mechanical properties of granite under corrosion acid and freeze–thaw cycles by uniaxial compression and freeze–thaw cycles.

However, the above tests were basically carried out under static water saturations, ignoring the erosion of underground rock engineering by longstanding flowing groundwater, and lacking in-depth discussion on the chemical damage mechanism and microscopic response mechanism (Zhao et al., 2017a; Liu et al., 2021b). In this article, based on the ion content of groundwater in the field, similar solutions with different pH values (pH = 7, 4, and 2) were mixed. Considering the scouring action of different velocity environments (v = 0, 150, and 300 mm·s^{-1}), we analyzed the granite surrounding rock of the tunnel at the water-rich area and chemical damage mechanism of microstructure, deformation characteristics, and physical properties under dynamic water environment. The results from this study are practically significant, which can provide some theoretical basis for the stability control of the rock mass of the bridge pile foundation bearing layer and tunnel surrounding rock at flowing groundwater.

2 LABORATORY TEST DESIGN

2.1 Sample and Solution Preparation

Granite was selected from the surrounding rock of the Gaoligongshan Tunnel Construction Project (see **Figures 1A,B**). According to the hydrogeological survey report of this section, groundwater in this area was abundant and weakly acidic (pH = 6.24), mainly containing cations such

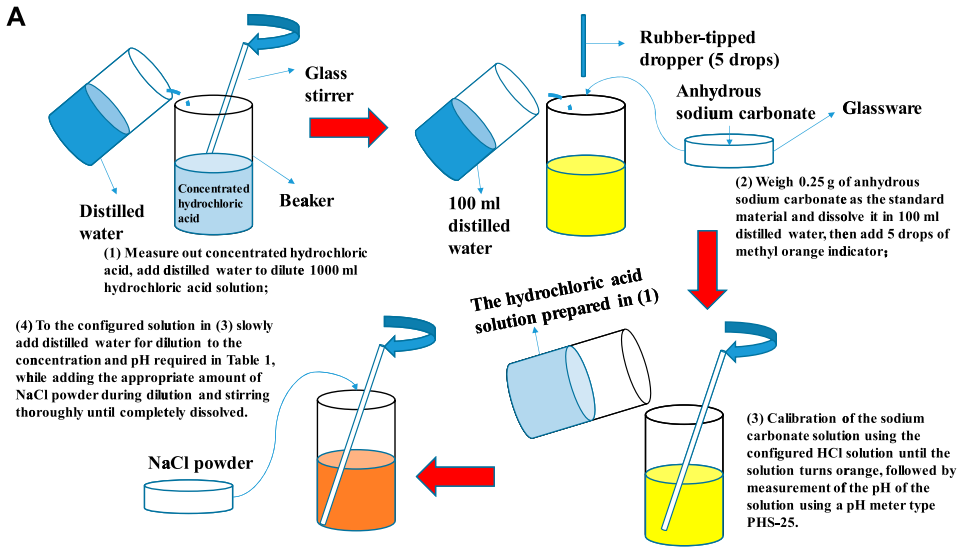

Diagram for configuration and calibration steps of acidic NaCl solution

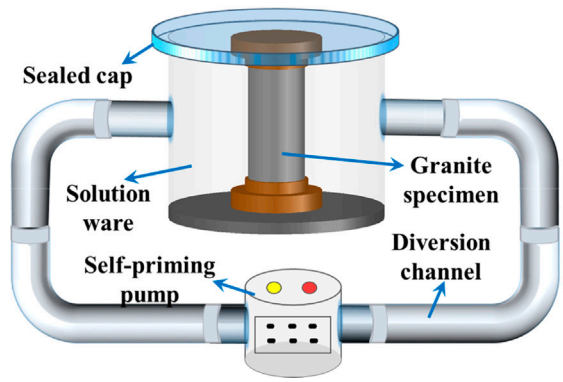

Schematic diagram of the water scouring device

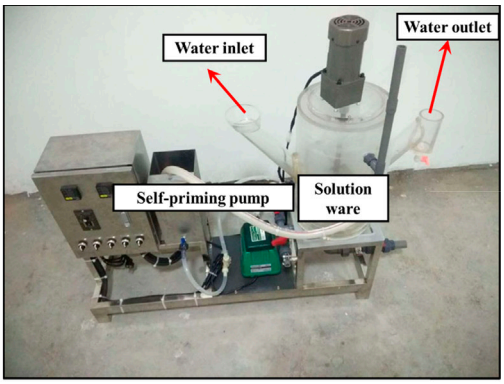

Water chemical solution scouring device

FIGURE 2 | Realization of dynamic water conditions. **(A)** Diagram for configuration and calibration steps of acidic NaCl solution. **(B)** Schematic diagram of the water scouring device. **(C)** Water chemical solution scouring device.

as Na^+, K^+, and Mg^{2+} and anions such as Cl^-, SO_4^{2-}, and HCO^{3-}. In addition, the annual average flow rate was about 150 mm·s^{-1}. Standard cylindrical samples of 50 × 100 mm (Zhao et al., 2016; Zhou et al., 2020; Dong et al., 2021) were prepared after drilling and coring of granite (see **Figure 1C**). The test synthesized the cations and anions with the largest percentage of groundwater content in the site and collocated NaCl solution with pH values of 7, 4, and 2 and a concentration of 0.01 mol·L^{-1}, respectively (see **Figure 2A**). Furthermore, three flow rate environments were simulated: v = 0, 150, and 300 mm·s^{-1}, and different immersion time nodes were set for follow-up measurements.

2.2 Dynamic Water Scouring Test Design

A hydro-chemical solution scouring device (see **Figures 2B,C**) was used to conduct scouring treatment tests on sandstone in solutions of different pH values and at different flow rates. The flushing device consists of a solution ware, a diversion channel, and a self-priming pump. The working principle is as follows: the solution ware is loaded into the solution, and the sample is placed and sealed, and the self-priming pump is operated. The solution circulates between the solution ware, the diversion channel, and the self-priming pump, and the flow rate of the solution is determined by the self-priming pump.

3 LABORATORY RESULTS AND ANALYSIS

3.1 Damage of Granite Under the Effect of Flowing Acid Solution

3.1.1 Analysis of Microstructure Changes

The macroscopic physical–mechanical state of granite is closely related to its own microstructure change (Zhao et al., 2017b;

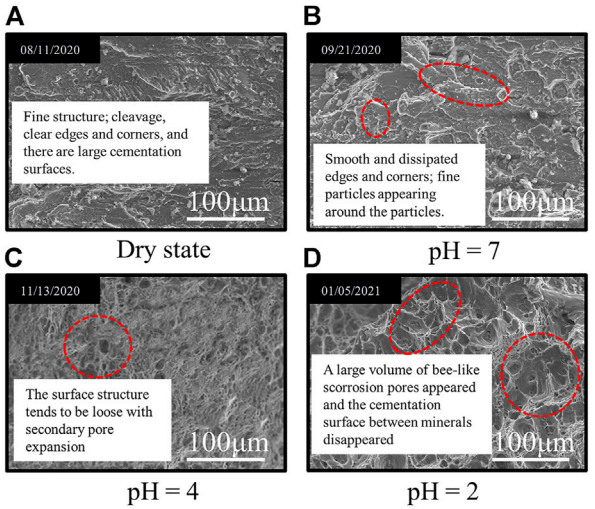

FIGURE 3 | Apparent scanning electron microscopy images of granite under different solution conditions for 49 days. **(A)** Dry state. **(B)** pH=7. **(C)** pH=4. **(D)** pH=2.

Dong et al., 2019; Zhou et al., 2019; Liu et al., 2021a). The test analyzed the differences in apparent morphological damage and pore structure of the samples before and after immersion treatment in acidic hydro-chemical solution with different flow rates and pH values through scanning with an electron microscope at a magnification of 500 times. The change in mineral composition near the pores was tracked using the electron energy spectrum analysis technology so as to explore the deterioration degree of granite microstructure under the effect of flowing acidic solution.

The surface scanning electron microscopy images of granite samples at different pH values under acidic solution environment (v = 0 mm·s^{-1}) for 49 days are shown in **Figure 3**.

After the samples were treated with hydro-chemical solution at various flow rates (pH = 6.24), the microscopic structure characterization (× 10^4 times) is shown in **Figure 4**.

As v = 150 mm·s^{-1}, the microstructure deterioration of the sample was more obvious than that in static water (see **Figure 4B**). Compared with the low velocity (v = 150 mm·s^{-1}), the micro-deterioration degree of the sample in the immersion environment with v = 300 mm·s^{-1} was stronger (see **Figure 4C**), but the deterioration degree was not as significant as the former.

Based on the groundwater flow rate of v = 150 mm·s^{-1} on site, the scanning electron microscopy at 10,000 times was observed under this flow rate with each solution rinsing for 49 days (see **Figure 5**).

Energy dispersive spectroscopy was used to measure the small area in the scanning image of electron microscope (the random three red crosses in **Figure 5**) to obtain the number of atoms and mass of the main components, and their average values are shown in **Table 1**. During saturation in NaCl acidic solution with pH = 4 and 2, a small amount of mineral composition in granite reacted with H^+ ions in the solution, causing some elements to dissolve and thereby break away from the rock, which resulted in the reduction of the content of metal elements such as Al, K, and Ca to different extents (see **Figure 5** and **Table 1**). On top of that, granite is a porous medium with certain absorbability, resulting in the increase of Na, Cl, and other elements after the effect of NaCl solution. Under the effect of NaCl solution with pH = 7 and distilled water, there was no obvious change in the content of main elements.

3.1.2 Porosity Change Analysis

Corrosion and hydrolysis will enable the active minerals to migrate with the groundwater and will increase the porosity,

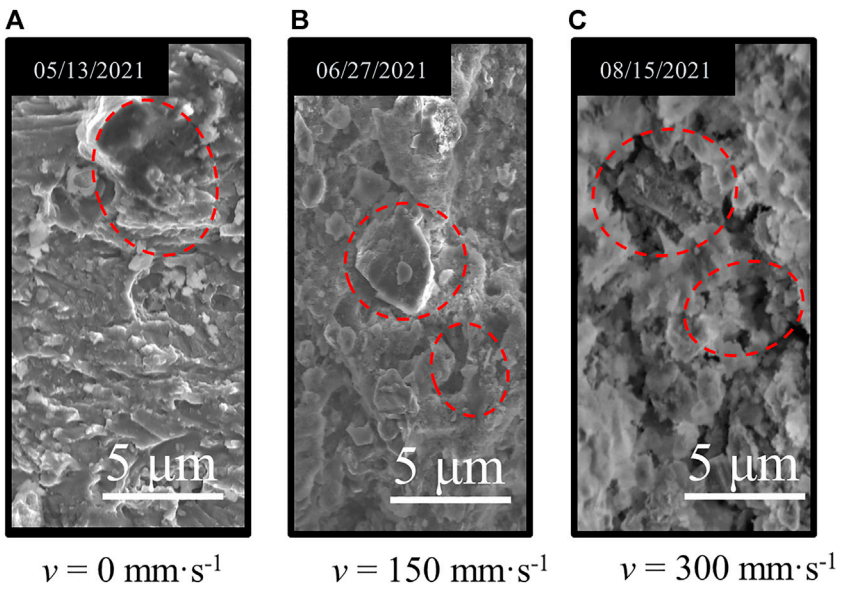

FIGURE 4 | Microstructural damage of granite immersed at different solution flow rates. **(A)** v = 0 mm·s^{-1} . **(B)** v = 150 mm·s^{-1}. **(C)** v = 300 mm·s^{-1}.

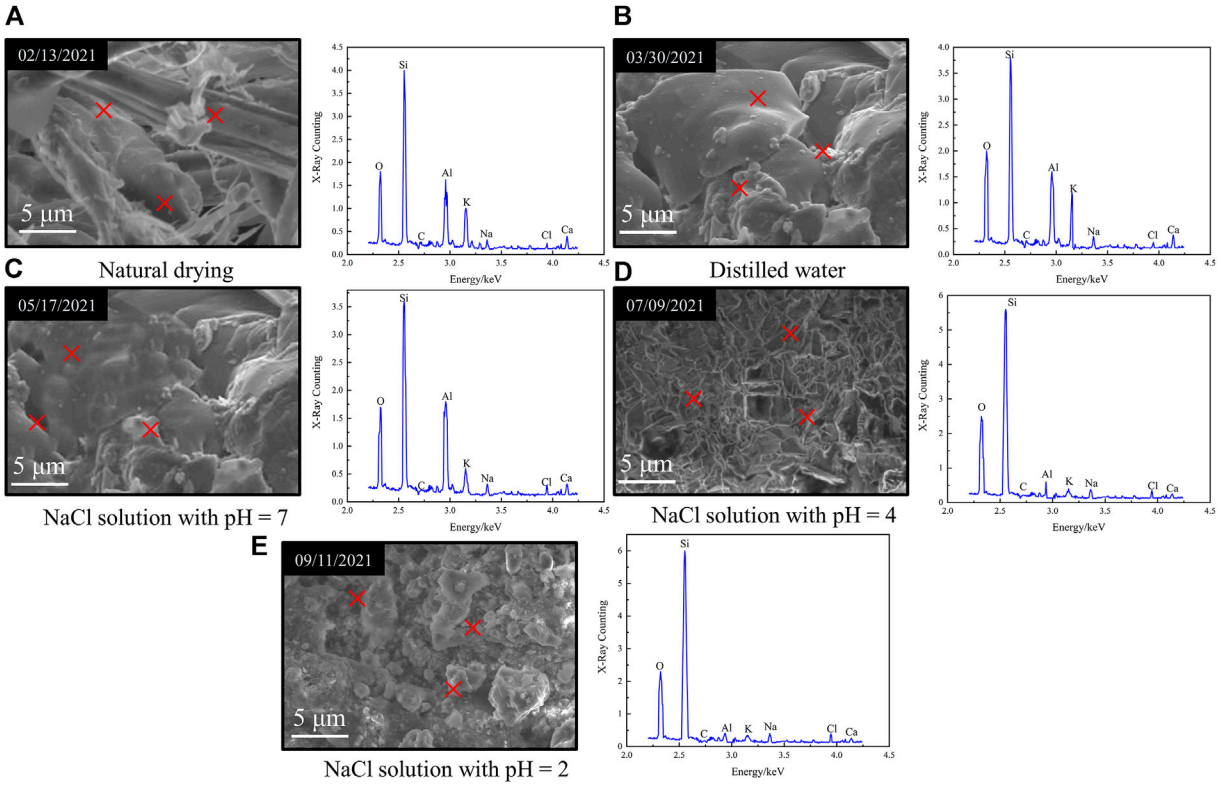

FIGURE 5 | Energy dispersive spectroscopy analysis of granite under the flow rate of v = 150 mm·s^{-1} with different aqueous chemical solutions for 49 days. **(A)** Natural drying. **(B)** Distilled water. **(C)** NaCl solution with pH=7. **(D)** NaCl solution with pH=4. **(E)** NaCl solution with pH=2

TABLE 1 | Comparison of the atomic number and mass content of the main components of granite under the flow rate of v = 150 mm·s^{-1} with different aqueous chemical solutions for 49 days.

Parameter		O	Si	C	Al	K	Na	Cl	Ca
Atom content/%	Dry	44.38	20.96	16.10	8.92	4.01	2.76	0.81	1.52
	Distilled water	41.52	15.87	19.32	6.05	5.23	4.06	1.10	2.26
	pH = 7	49.07	24.03	11.95	7.14	2.96	3.24	1.73	1.36
	pH = 4	51.05	15.31	11.01	6.40	3.33	4.56	1.99	1.00
	pH = 2	42.26	24.72	21.23	2.46	2.60	3.01	2.69	0.60
Mass content/%	Dry	34.48	29.46	9.23	11.85	7.13	3.23	1.30	3.06
	Distilled water	31.78	22.05	14.66	10.06	9.45	4.51	3.84	4.45
	pH = 7	39.06	30.43	8.06	9.30	4.98	3.72	3.40	2.75
	pH = 4	43.09	18.99	5.31	14.10	7.20	4.99	2.83	1.56
	pH = 2	32.52	33.93	15.41	3.74	3.96	2.88	5.51	1.00

which will impact on the pore pressure and permeability of the granite (Zhao et al., 2021a; Dong et al., 2022). The porosity of the sample subjected to acidic solution was determined by the pycnometer bottle test method (Grgic et al., 2022) and nuclear magnetic resonance (NMR) technique. Three samples were selected for each solution with different pH values and flow rates. **Figure 6** shows the test results. Porosity was calculated as follows (Zhao et al., 2019):

$$n = \left(\rho_g - \rho_d\right)/\rho_g \times 100\%, \quad (1)$$

where n is the porosity of the rock sample, ρ_g is the grain density of the rock sample, and ρ_d is the dry density of the sample.

Figure 6 indicates that the porosity of the sample increases exponentially with the decrease in pH of the acid solution. Compared to the dry sample, the porosity of the samples under various acidic solution saturations (pH value from high to low) with the flow rate of 0 had smaller variations, and the growth rates were 3.5, 9.4, 30.7, and 45.9%, respectively (see **Figure 6A**). The average porosity of the treated samples increased by 4.5, 10.8, 34.1, and 48.3%, respectively, under

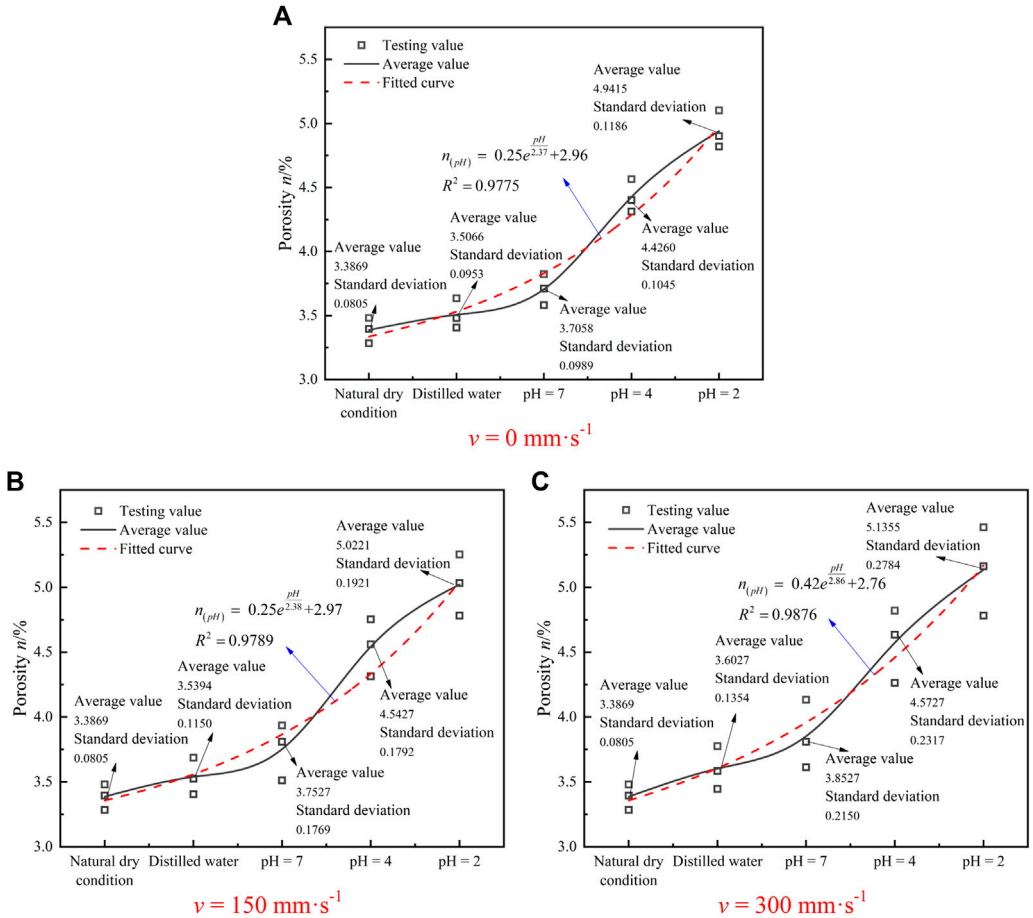

FIGURE 6 | Porosity change diagram of granite samples under different flow rates of acid solution. **(A)** v = 0 mm·s^{-1} . **(B)** v = 150 mm·s^{-1}. **(C)** v = 300 mm·s^{-1}.

different saturations with v = 150 mm·s^{-1} (see **Figure 6B**). As v = 300 mm·s^{-1}, the average porosity increases with 6.4, 13.8, 35, and 51.6%, respectively (see **Figure 6C**). In addition, compared with natural drying and distilled water, the porosity of samples measured by acidic solution had more obvious dispersion, and the porosity dispersion of v = 150 mm·s^{-1} was significantly lower than that of v = 300 mm·s^{-1}. There are two reasons: one is the heterogeneity of the rock sample, and the other is the selective difference of chemical action on the rock. Given this, the dynamic solution environment has a certain role in promoting the dispersion of rock porosity, and when the hydro-chemical solution in which the rock mass is located has a higher flow rate, the effect is more obvious.

3.2 Deterioration and Aging Characteristics of Granite Under Flowing Acid Solution

Physical parameters such as the sample mass and the pH value of the immersed solution were determined with 7 days as the time node during the saturation, and measurements were carried out every day during the first 5 days. After the test, the ion chromatography was used to measure and analyze the ion composition and concentration of the chemical solution.

3.2.1 Evolution of Mass Loss

To reduce the random error of test results, the sample was ventilated for 0.5 h to ensure the same test condition. Under the effect of water and various flow rates of acidic aqueous chemical solution, the mass of the sample was reduced inordinately. The mass damage level of granite was described by the mass loss factor D_t:

$$D_t = (m_0 - m_t)/m_0 \times 100\%. \quad (2)$$

In **Eq. 2**, m_0 is the original mass of the sample and m_t is the mass of the sample at time t.

Figure 7 shows the mass loss aging characteristic curves of granite after saturation in four kinds of dynamic aqueous chemical solutions.

As seen in **Figure 7**, the mass loss degree of the sample increased with the decrease in the pH value of the hydro-chemical solution. Under saturation at the same pH value, the mass loss degree of the sample with v = 0 mm·s^{-1} was significantly lower than that of the sample with v =150 mm·s^{-1}. However, the

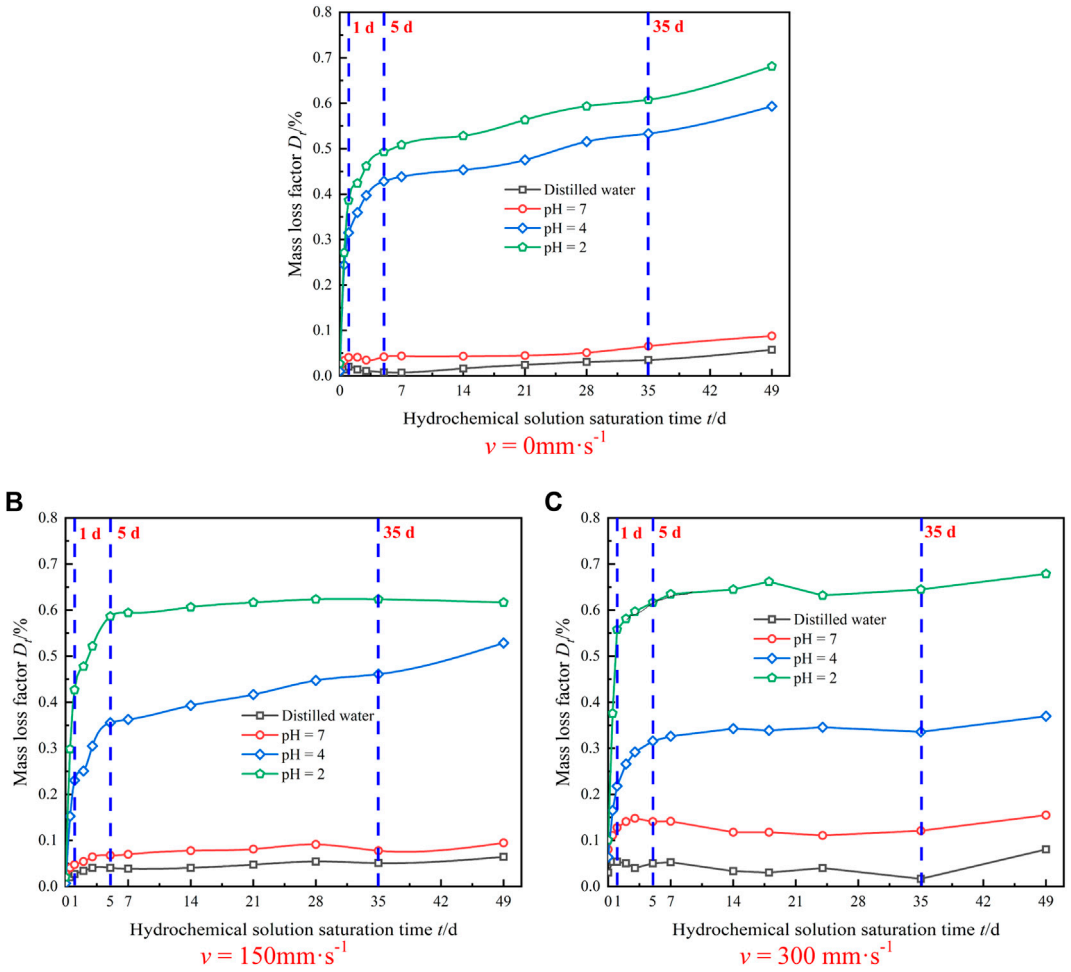

FIGURE 7 | Time-dependent variation curve of rock mass loss during the test process. **(A)** v = 0 mm·s^{-1} . **(B)** v = 150 mm·s^{-1}. **(C)** v = 300 mm·s^{-1}.

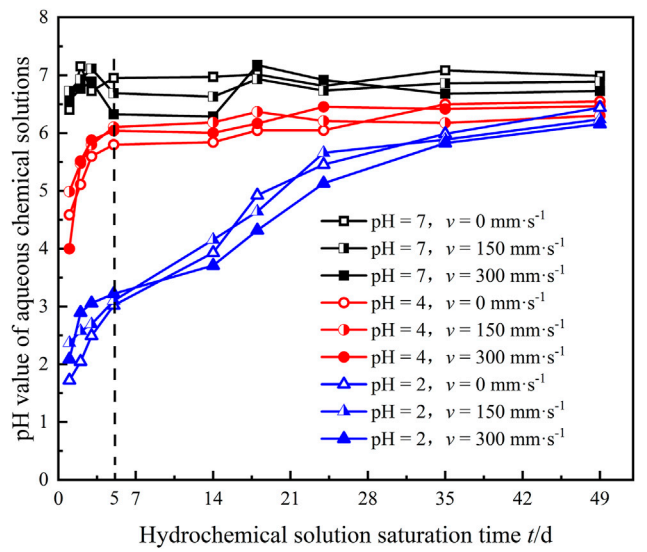

FIGURE 8 | Time-dependent curve of the aqueous chemical solution pH value in the test process.

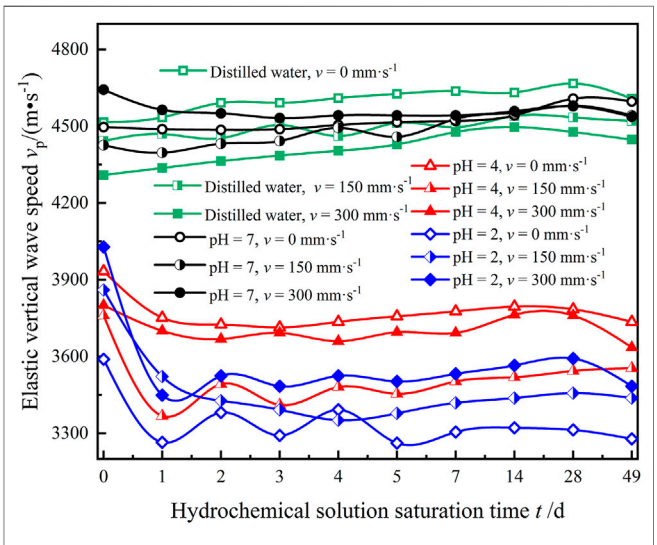

FIGURE 9 | Time-dependent variation curve of the granite elastic vertical wave speed of granite during the test process.

TABLE 2 | Variation in elastic longitudinal wave velocity of granite by different hydro-chemical solutions.

Test environment	Velocity/(mm·s^{-1})	v_{sp}/(m·s^{-1})	v_{fp}/(m·s^{-1})	E_p/%
Distilled water	0	4,516	4,608	−2.04
	150	4,443	4,521	−1.77
	300	4,310	4,448	−3.20
pH = 7	0	4,497	4,597	−2.23
	150	4,426	4,543	−2.63
	300	4,643	4,537	2.27
pH = 4	0	3,934	3,736	5.02
	150	3,760	3,555	5.47
	300	3,801	3,636	4.34
pH = 2	0	3,590	3,279	8.67
	150	3,861	3,438	10.94
	300	4,028	3,484	13.51

mass loss degree of the sample with v = 300 mm·s^{-1} was slightly higher than that of the sample with v = 150 mm·s^{-1}. In the pH = 2 acidic solution, the granite samples reacted strongly in the acidic chemical solution with various flow rates at the initial stage (0 ~ 5 days), and the active minerals dissolved and formed some bubbles. The mass loss rate was the highest (0.487, 0.574, and 0.686%, respectively). As the time went on, the chemical reaction rate gradually slowed down until it became steady.

3.2.2 Law of pH Change With time

As mentioned earlier, the initial pH of the aqueous solution is the key factor to influence the corrosion mechanism of granite. The time, phenomenon, and degree of chemical reaction of the sample during the test can be directly mirrored by the change in solution pH (Miao et al., 2016). **Figure 8** shows the characteristic curve of the pH value with time during the immersion of the sample in acidic solution at various flow rates. In **Figure 8**, the granite sample produced a weak chemical reaction in the NaCl solution immersion with pH = 7, and the measured pH value of the solution ranged from 6.29 to 7.18,

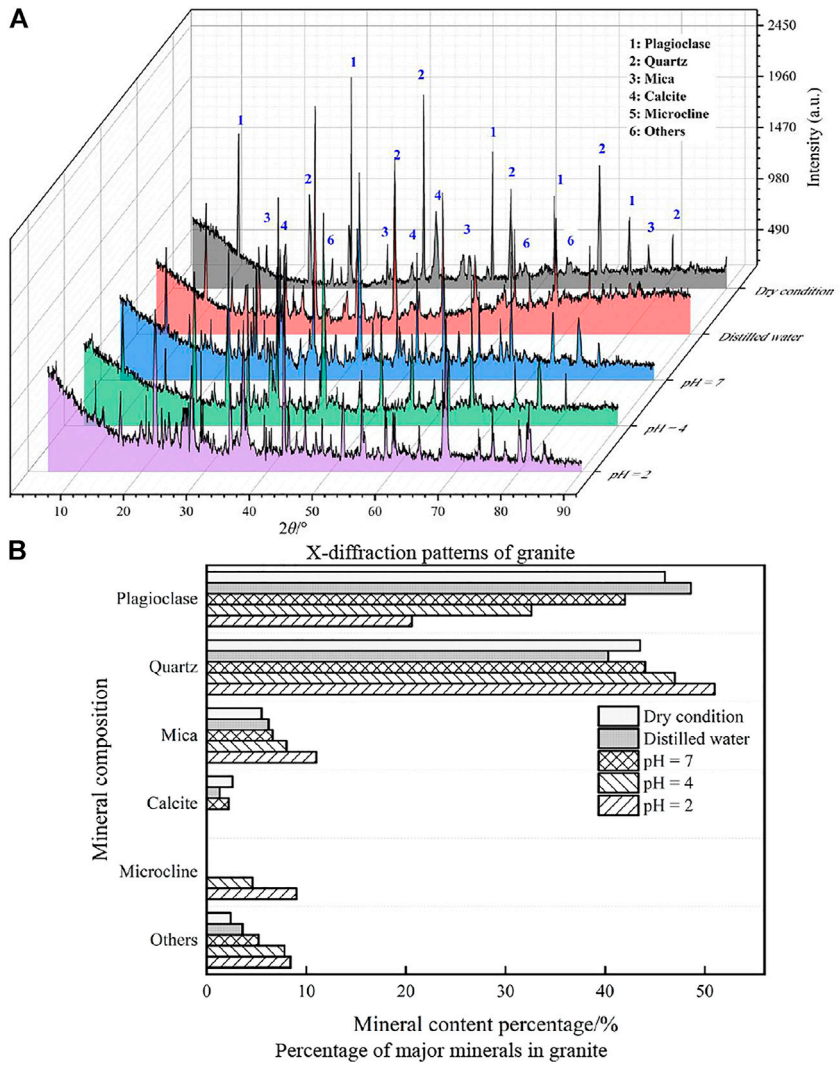

FIGURE 10 | X-ray diffraction results of granite mineral composition before and after different treatment. **(A)** X-diffraction patterns of granite. **(B)** Mineral content percentage/% percentage of major minerals in granite.

TABLE 3 | Content of main mineral components of granite before and after immersion in different aqueous chemical solutions.

Test environment	Mass percentage of mineral content/%					
	Microcline	Calcite	Mica	Quartz	Plagioclase	Others
Dry condition	—	2.6	5.5	43.5	46	2.4
Distilled water	—	1.3	6.2	40.3	48.6	3.6
pH = 7	—	2.2	6.6	44	42	5.2
pH = 4	4.6	—	8	47	32.6	7.8
pH = 2	9	—	11	51	20.6	8.4

TABLE 4 | Contents of the main compounds and chemical elements in granite before and after the action of different hydro-chemical solutions.

Test environment	Mass percentage of the compound and element content/%										
	SiO_2	Al_2O_3	C	CaO	K_2O	Na_2O	Fe_2O_3	Cl	N	TiO_2	MgO
Dry condition	62.10	17.20	9.40	3.49	3.33	2.87	0.91	0.69	0.29	0.27	0.19
Distilled water	64.20	15.00	10.13	1.86	3.16	3.99	0.87	0.10	0.22	0.12	0.9
pH = 7	58.20	14.90	8.02	1.43	3.13	3.37	0.67	0.34	0.46	0.29	0.35
pH = 4	65.90	11.90	10.59	0.92	3.01	2.52	0.62	0.51	0.49	0.20	0.26
pH = 2	73.50	8.80	11.60	0.60	2.50	0.50	0.60	1.00	0.60	0.30	0.10

which reflected a good stability. At the beginning of immersion, the H^+ in the solution and the new active minerals in the sample continually reacted on the granite surface. After corrosion, the active minerals moved with water flow or dissolved in the solution, and the pH value of the solution changed obviously. When v = 300 mm·s^{-1}, the change rates of pH = 7, 4, and 2 after soaking for 5 days were −0.4, 33.8, and 38.9%, respectively. After soaking for 5–6 days, the NaCl solution with pH = 4 was almost stable, but the change rate of the NaCl solution with pH = 2 decreased gradually from 26%/d (0 ~ 5 days) to 5.7%/d (5 ~ 49 days). Upon saturation, the pH values of the three aqueous chemical solutions were basically neutral. "Water–rock Interaction" (WRI) mainly manifests as hydraulic and physical actions, and the chemical corrosion action is nearly inactive.

3.2.3 Time-Dependent Variation in Elastic Vertical Wave Velocity

The physical properties of rock determine the spread rate of ultrasonic waves in the rock to a certain extent (Cherblanc et al., 2016; Weng et al., 2020). The acoustic wave of granite was measured by an acoustic wave tester at each time node of acid solution treatment so as to obtain the aging regularity of granite elastic vertical wave velocity under flowing acidic solution. **Figure 9** shows the measurement result.

From **Figure 9**, it can be seen that there was no obvious fluctuation in the granite elastic vertical wave velocity and the stability was good in the initial stage of the test, when the granite was immersed in water and NaCl solution with pH = 7. The elastic vertical wave velocity (v_p) of granite samples decreased significantly in acidic solution with pH of 4 and 2, and it decreased by 9.1, 8.8, and 14.4% in NaCl solution with pH of 2 with flow rates of v = 0, 150, and 300 mm·s^{-1}, respectively. Then, there were fluctuations, but the fluctuations gradually slowed down over time, and the fluctuation cycle presented an increasing trend over time; v_p hardly changed after 5 ~ 7 days of immersion. As the immersion environment was water and NaCl solution with pH = 7, v_p of a few specimens also fluctuated slightly, but it showed a smooth rise overall.

Based on the large quantity of research and tests (Ha et al., 2015; Hao et al., 2015; Cai et al., 2016; Dong and Luo, 2022), the analysis is as follows: (1) at the initial stage of immersion, the active oxide contained in the sample in the ideal state reacted with H^+ in the acidic solution, resulting in dissolution pores, an increase in porosity, and a decrease in wave velocity; the rate of chemical reaction gradually flattened as the pH value of solution became neutral, and the saturation rate of rock increased gradually due to product precipitation and water absorption. The v_p of the sample witnessed a small increase until it became stable. However, owing to the heterogeneity of granite and its potential micro-fissures, such micro-fractures may continue to develop, expand, or initiate new fissures under the effect of acidic solution. Compared with the environment with v = 0 mm·s^{-1}, the fluctuation of v_p was significantly enhanced due to the water absorption and the WRI brought by low and high speed immersion environment. Meanwhile, under NaCl solution with pH = 7, the pores of rocks gradually reached saturation because of the absorption of water molecules, whereby v_p slowly increased. (2) The saturation of the samples was decreased after extraction and drying for 49 days after immersion. Comparing the saturation of water for 28 days, the measured v_p of all samples decreased. E_P was used to characterize the variation in elastic vertical wave velocity, and its expression is as follows:

$$E_p = \left(v_{sp} - v_{fp}\right)\Big/ v_{sp} \times 100\%. \quad (3)$$

In **Eq. 3**, v_{sp} is the original elastic vertical wave velocity and v_{fp} is the elastic P-wave velocity after the test.

The calculation of E_p of the sample treated with acidic solution is shown in **Table 2**. In **Table 2**, the rock saturation increased

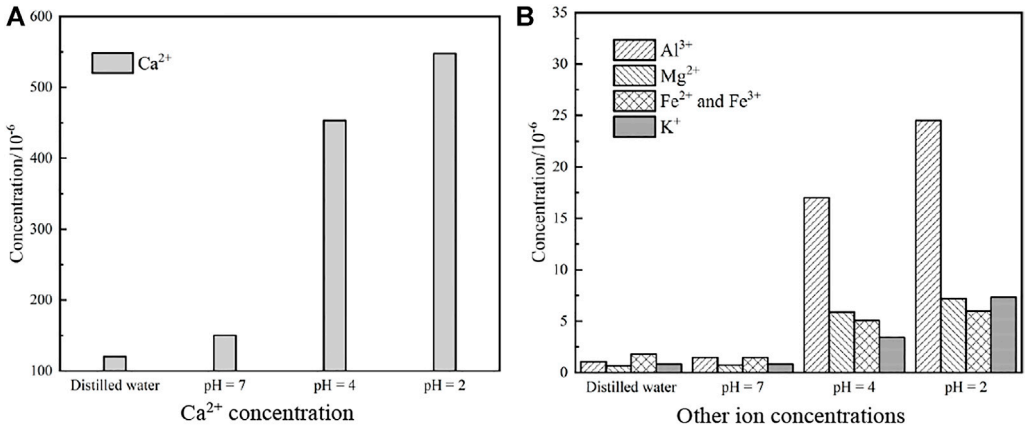

FIGURE 11 | Detection results of ion concentration in aqueous chemical solution after saturation. **(A)** Ca^{2+} concentration. **(B)** Other icon concentration.

after the WRI, but its physical properties deteriorated. The causes are as follows: the reaction of granite active minerals with H^+ in the solution enables the rock to be corroded and dissolved, the whole structure appears fissured, and the porosity increases, which leads to the decrease in v_p.

4 DISCUSSION ON THE MECHANISM OF FLOWING ACIDIC SOLUTION

4.1 Variation in Mineral Composition of Granite

After 49 days of the groundwater velocity (v = 150 mm·s^{-1}) test at the sampling site, the mineral composition profiles of the water and the samples before and after treatment with each acidic solution were obtained by X-ray diffraction phase analysis (see **Figure 10A**). The mineral composition distribution of the sample was obtained using Jade software (see **Figure 10B**) to investigate the mineral composition and physical properties of the granite under the effect of acid solution. The mineral content of the sample is shown in **Table 3**. In order to improve the accuracy of the quantitative analysis of the X-ray diffraction results, the contents of the compounds and elements in all granite samples were determined by a semi-quantitative test (see **Table 4**).

According to **Figure 10** and **Table 3**, calcite and plagioclase increase with acidity, and the contents were reduced to some extent. The calcite was completely dissolved at pH = 4 and 2, but the content of mica and quartz was obviously increased, and new mineral microcline and other impurities were formed in the reaction process.

4.2 Variation in Ion Concentration in Test Solution

When reactive minerals in rocks react with chemical solutions, some elements in rocks enter the solution in the form of ions, and the salinity of the solution changes accordingly. In order to explore the damage mechanism of flowing acidic solution on granite, we analyzed the chemical compounds and mineral components involved in the hydro-chemical reaction of granite, discussed the mode and degree of water–rock interaction, and detected the soaked chemical solution by ion chromatography. The results are shown in **Figure 11**.

Figure 11 shows that H^+ in the immersion solution reacts with mineral components such as calcite and plagioclase in granite to form cations such as Fe^{2+}, Fe^{3+}, Ca^{2+}, Al^{3+}, Mg^{2+}, K^+, and Na^+. Different mineral components had different perceptions of chemical environment, leading to significant differences in the concentration of each ion in the chemical solution. Moreover, the acidic chemical solution contains 0.01 mol·L^{-1} NaCl solution, and the amount of Na^+ precipitated out of granite during the reaction was far less than that of the test solution, so the content variations of Na^+ are not discussed.

In the NaCl solution with pH = 7 and distilled water, there was almost no chemical reaction of granite, and only some silicate and carbonate minerals were hydrolyzed, which led to a slight increase in metal cation concentration. After 49 days of treatment with NaCl solution with pH = 4, the concentration of all metal cations substantially increased, which indicated that the chemical reaction between H^+ in solution and active granite minerals became more and more intense. NaCl solution with pH = 2 for 49 days contained 547.83 × 10^{-6} of Ca^{2+}, 7.19 × 10^{-6} of Mg^{2+}, and 24.52 × 10^{-6} of Al^{3+}, indicating that the precipitated ion concentration was mainly controlled by the initial pH of the chemical solution.

4.3 Chemical Reaction and Mechanism of Granite

4.3.1 Chemical Reaction Process of Acidic Solution With Granite

Tables 3 and **4** show that the mineral composition of granite includes a small amount of mica and calcite and a large amount of plagioclase and quartz. These minerals are easily corroded and hydrolyzed in acidic solutions, and the reaction between calcite and plagioclase and acid solution is more intense, while the reaction between quartz and acid solution is weak. The chemical reactions between acidic solution and the mineral components of the granite are as follows:

1) Reaction between few mica and H^+ ions in solution (Liu et al., 2018):

$$KAl_3Si_3O_{10}(OH)_2 + 10H^+ \rightarrow 3Al^{3+} + 3SiO_2 + 6H_2O + K^+ \quad (4)$$

2) Significant reaction between calcite and H^+ ions in solution (Zhao et al., 2021c):

$$CaCO_3 + 2H^+ \rightarrow Ca^{2+} + H_2O + CO_2 \quad (5)$$

3) Plagioclase, albite, orthoclase, and anorthite as a series of components react with H^+ ions in acidic solution as follows:

$$NaAlSi_3O_8 + 4H^+ \rightarrow Al^{3+} + 3SiO_2 + 2H_2O + Na^+ \quad (6)$$

$$KAlSi_3O_8 + 4H^+ \rightarrow Al^{3+} + 3SiO_2 + 2H_2O + K^+ \quad (7)$$

$$CaAl_2Si_2O_8 + 8H^+ \rightarrow 2Al^{3+} + 2SiO_2 + 4H_2O + Ca^{2+} \quad (8)$$

4) Insignificant hydrolysis reaction occurs after quartz comes into contact with water:

$$SiO_2 + 2H_2O \rightarrow H_4SiO_4 \quad (9)$$

Combined with **Table 3** and **Figure 10A**, we can see that after saturated in NaCl solution with pH = 4 and 2, the calcite in the sample was almost completely hydrolyzed, the content of plagioclase decreased significantly, and microcline was produced. The reaction between acidic solution and mica, quartz, and other mineral reaction was not obvious; hence, the material consumption was less, and the mass percentage of Ca^{2+} precipitated into the solution increased slightly. The micro-mineral composition of granite is easy to change under the effect of acid chemical solution, but the change of mineral composition of the sample is relatively small in the pH = 7 NaCl solution and distilled water.

4.3.2 Chemical Mechanism of Granite in Flowing Acidic Solution

1) Chemical mechanism

Based on the principles of chemical kinetics (Lin et al., 2020), the chemical reactions between the key compounds of granite (see **Table 4**) and the acidic solution are as follows:

$$CaO + 2H^+ == Ca^{2+} + H_2O \quad (10)$$

$$Al_2O_3 + 6H^+ == 2Al^{3+} + 3H_2O \quad (11)$$

$$MgO + 2H^+ == Mg^{2+} + H2O \quad (12)$$

$$Fe_2O_3 + 6H^+ == 2Fe^{3+} + 3H_2O \quad (13)$$

$$K_2O + 2H^+ == 2K^+ + H_2O \quad (14)$$

$$Na_2O + 2H^+ == 2Na^+ + H_2O \quad (15)$$

As can be seen from **Table 4** and **Figure 11**, the content of active compounds such as CaO, MgO, Al_2O_3, Fe_2O_3, Na_2O, K_2O, and so on decreased after the flowing acidic solution, which led to the increase in the concentration of Ca^{2+}, Mg^{2+}, Al^{3+}, Fe^{3+}, K^+, and other metal cations in the solution. Beyond that, in **Table 4** and **Figure 11**, different mineral components in rock samples had different sensitivities in acidic environment: the more acidic the environment, the greater the reaction degree of Al_2O_3 and CaO. In addition, the concentration of plasma such as Al^{3+} and Ca^{2+} increased greatly in the solution after the reaction stopped. The chemical reaction between water and NaCl solution with pH = 7 was weak, and the mineral content in granite was hardly invariant.

Therefore, rock and mineral particles produce various "Ion Exchange (IEX)" under acidic solution, which weakens the compactness of grain skeleton and causes the deterioration of its physical and mechanical properties. Besides, some ions escape with the flowing solution, resulting in the increase of pore size and quantity of granite internal pores, then occurring to the accumulation to form defect morphology, and finally changing the microscopic characterization. The lower the pH value is, the more significant the chemical damage is.

2) Physical effects

The scour and dissolution of the flowing acidic solution reduce the cementation between the granite mineral particles and weaken the friction between the mineral particles. In the meantime, the pore pressure caused by water entering the sample impairs the intergranular compressive stress and then produces a splitting effect on the micropores.

In summary, the chemical disequilibrium between rock minerals and acid solution contributes to an irreversible thermodynamic process, and the physical and chemical reactions between rock and groundwater lead to the deterioration and damage of rock microstructure and mineral composition, which generates hydrolysis and dissolution of primary minerals to form new minerals and components. Moreover, the crystal skeleton and cemented structure of rock particles degenerate, the porosity expands, the rock porosity increases, and the strength decreases. Therefore, the coupling effect between the composition of hydro-chemical solution and the mineral composition, and the overall structure (such as cracks and pores) of rock controls the deterioration mechanism of "water–rock interaction" (WRI), and the microstructure and meso-composition of granite change accordingly.

5 CONCLUSION

In light of the aforementioned work, the main conclusions of this study are as follows:

1) Combined with the SEM and XRD analysis results, the microscopic structure, mineral composition content, and defect morphology of the granite samples change after being treated with various flowing acidic solutions. The initial pH value of solution is the main determinant of chemical corrosion degradation.
2) By observing the test results of damage aging characteristics of granite, granite tends to be stable after acidic solution corrosion for a period of time. At this time, the damage aging curves of sample mass, elastic vertical wave velocity, and chemical solution pH value gradually stabilize. After the granite was soaked in NaCl solution with pH = 2 for 49 days, compared with the low speed ($v = 150\ mm{\cdot}s^{-1}$, approximate field velocity), the mass damage factor in high speed increased by 8.8% and the elastic vertical wave velocity decreased by 19.3%.

3) The granite secondary porosity increases, the specific surface area increases, the structure tends to be loose, the porosity increases, and the dispersion becomes more obvious after the effect of the flowing acidic solution. The lower the pH value of the solution, the higher the velocity, and the aforementioned variations are more significant.
4) At an approximate in field velocity (v =150 mm·s^{-1}), the chemical reaction process between the rock and the acidic solution and the chemical damage mechanism of the rock are determined by the composition and properties of the aquatic chemical solution, as well as the coupling effect between rock mineral composition and overall structure (such as cracks and pores).

DATA AVAILABILITY STATEMENT

The original contributions presented in the study are included in the article/Supplementary Material, further inquiries can be directed to the corresponding author.

AUTHOR CONTRIBUTIONS

Methodology and funding acquisition: WC, WW, and YZ. Software: QW and SX. Data curation and formal analysis: YZ and XW. Visualization: LW. Supervision: HH. All authors have read and agreed to the published version of the manuscript.

FUNDING

This research was funded by the National Natural Science Foundation of China (51774118, 51774132) and the Natural Science Foundation of Hunan Province (2021JJ30265).

ACKNOWLEDGMENTS

We thank Jie Liu, Min Wang, and Xiaoyu Tang for useful discussions and for early contributions to the project and the reviewers for their very helpful and inspiring comments.

REFERENCES

Bai, B., Long, F., Rao, D., and Xu, T. (2017). The Effect of Temperature on the Seepage Transport of Suspended Particles in a Porous Medium. *Hydrol. Process.* 31 (2), 382–393. doi:10.1002/hyp.11034

Bai, B., Nie, Q., Zhang, Y., Wang, X., and Hu, W. (2021). Cotransport of Heavy Metals and SiO2 Particles at Different Temperatures by Seepage. *J. Hydrology* 597, 125771. doi:10.1016/j.jhydrol.2020.125771

Cai, Y. Y., Yu, J., Fu, G. F., and Li, H. (2016). Experimental Investigation on the Relevance of Mechanical Properties and Porosity of Sandstone after Hydrochemical Erosion. *J. Mt. Sci.* 13 (11), 2053–2068. doi:10.1007/s11629-016-4007-2

Chen, Y., Xiao, P., Du, X., Wang, S., Fernandez-Steeger, T. M., and Azzam, R. (2021). Study on Damage Constitutive Model of Rock under Freeze-Thaw-Confining Pressure-Acid Erosion. *Appl. Sci.* 11 (20), 9431. doi:10.3390/app11209431

Cherblanc, F., Berthonneau, J., Bromblet, P., and Huon, V. (2016). Influence of Water Content on the Mechanical Behaviour of Limestone: Role of the Clay Minerals Content. *Rock Mech. Rock Eng.* 49 (6), 2033–2042. doi:10.1007/s00603-015-0911-y

Dong, L.-j., Zhou, Y., Deng, S.-j., Wang, M., and Sun, D.-y. (2021). Evaluation Methods of Man-Machine-Environment System for Clean and Safe Production in Phosphorus Mines: A Case Study. *J. Cent. South Univ.* 28 (12), 3856–3870. doi:10.1007/s11771-021-4890-8

Dong, L., and Luo, Q. (2022). Investigations and New Insights on Earthquake Mechanics from Fault Slip Experiments. *Earth-Science Rev.* 228, 104019. doi:10.1016/j.earscirev.2022.104019

Dong, L., Sun, D., Shu, W., and Li, X. (2020). Exploration: Safe and Clean Mining on Earth and Asteroids. *J. Clean. Prod.* 257, 120899. doi:10.1016/j.jclepro.2020.120899

Dong, L., Tao, Q., Hu, Q., Deng, S., Chen, Y., Luo, Q., et al. (2022). Acoustic Emission Source Location Method and Experimental Verification for Structures Containing Unknown Empty Areas. *Int. J. Min. Sci. Technol.* 32 (3), 487–497. doi:10.1016/j.ijmst.2022.01.002

Dong, L., Tong, X., Li, X., Zhou, J., Wang, S., and Liu, B. (2019). Some Developments and New Insights of Environmental Problems and Deep Mining Strategy for Cleaner Production in Mines. *J. Clean. Prod.* 210, 1562–1578. doi:10.1016/j.jclepro.2018.10.291

Grgic, D., Al Sahyouni, F., Golfier, F., Moumni, M., and Schoumacker, L. (2022). Evolution of Gas Permeability of Rock Salt under Different Loading Conditions and Implications on the Underground Hydrogen Storage in Salt Caverns. *Rock Mech. Rock Eng.* 55 (2), 691–714. doi:10.1007/s00603-021-02681-y

Ha, Y. D., Lee, J., and Hong, J.-W. (2015). Fracturing Patterns of Rock-like Materials in Compression Captured with Peridynamics. *Eng. Fract. Mech.* 144, 176–193. doi:10.1016/j.engfracmech.2015.06.064

Hao, R.-q., Li, J.-t., Cao, P., Liu, B., and Liao, J. (2015). Test of Subcritical Crack Growth and Fracture Toughness under Water-Rock Interaction in Three Types of Rocks. *J. Cent. South Univ.* 22 (2), 662–668. doi:10.1007/s11771-015-2568-9

Huang, Z., Zeng, W., Gu, Q., Wu, Y., Zhong, W., and Zhao, K. (2021). Investigations of Variations in Physical and Mechanical Properties of Granite, Sandstone, and Marble after Temperature and Acid Solution Treatments. *Constr. Build. Mater.* 307, 124943. doi:10.1016/j.conbuildmat.2021.124943

Huo, R., Li, S., and Ding, Y. (2018). Experimental Study on Physicochemical and Mechanical Properties of Mortar Subjected to Acid Corrosion. *Adv. Mater. Sci. Eng.* 2018, 11. doi:10.1155/2018/3283907

Li, S., Wu, Y., Huo, R., Song, Z., Fujii, Y., and Shen, Y. (2021). Mechanical Properties of Acid-Corroded Sandstone under Uniaxial Compression. *Rock Mech. Rock Eng.* 54 (1), 289–302. doi:10.1007/s00603-020-02262-5

Lin, Y., Zhou, K., Li, J., Ke, B., and Gao, R. (2020). Weakening Laws of Mechanical Properties of Sandstone under the Effect of Chemical Corrosion. *Rock Mech. Rock Eng.* 53 (4), 1857–1877. doi:10.1007/s00603-019-01998-z

Liu, H., Zhu, W., Yu, Y., Xu, T., Li, R., and Liu, X. (2020). Effect of Water Imbibition on Uniaxial Compression Strength of Sandstone. *Int. J. Rock Mech. Min. Sci.* 127, 104200. doi:10.1016/j.ijrmms.2019.104200

Liu, X., Liang, Z., Zhang, Y., Liang, P., and Tian, B. (2018). Experimental Study on the Monitoring of Rockburst in Tunnels under Dry and Saturated Conditions Using AE and Infrared Monitoring. *Tunn. Undergr. Space Technol.* 82, 517–528. doi:10.1016/j.tust.2018.08.011

Liu, X., Wu, L., Zhang, Y., Liang, Z., Yao, X., and Liang, P. (2019). Frequency Properties of Acoustic Emissions from the Dry and Saturated Rock. *Environ. Earth Sci.* 78 (3), 67. doi:10.1007/s12665-019-8058-x

Liu, X., Wu, L., Zhang, Y., and Mao, W. (2021a). Localized Enhancement of Infrared Radiation Temperature of Rock Compressively Sheared to Fracturing Sliding: Features and Significance. *Front. Earth Sci.* 9, 756369. doi:10.3389/feart.2021.756369

Liu, X., Wu, L., Zhang, Y., Wang, S., Yao, X., and Wu, X. (2021b). The Characteristics of Crack Existence and Development during Rock Shear Fracturing Evolution. *Bull. Eng. Geol. Environ.* 80 (2), 1671–1682. doi:10.1007/s10064-020-01997-3

Miao, S., Cai, M., Guo, Q., Wang, P., and Liang, M. (2016). Damage Effects and Mechanisms in Granite Treated with Acidic Chemical Solutions. *Int. J. Rock Mech. Min. Sci.* 88, 77–86. doi:10.1016/j.ijrmms.2016.07.002

Wang, S., Chen, Y., Ni, J., Liu, G., Fernández-Steeger, T. M., and Xu, C. (2021). Mechanical Characteristics and Mechanism of Granite Subjected to Coupling Effect of Acidic Corrosion and Freeze-Thaw Cycles. *J. Earth Sci.* 32 (5), 1202–1211. doi:10.1007/s12583-021-1414-2

Weng, L., Wu, Q.-h., Zhao, Y.-l., and Wang, S.-m. (2020). Dynamic Response and Failure of Rock in Initial Gradient Stress Field under Stress Wave Loading. *J. Cent. South Univ.* 27 (3), 963–972. doi:10.1007/s11771-020-4344-8

Xie, S. Y., Shao, J. F., and Xu, W. Y. (2011). Influences of Chemical Degradation on Mechanical Behaviour of a Limestone. *Int. J. Rock Mech. Min. Sci.* 48 (5), 741–747. doi:10.1016/j.ijrmms.2011.04.015

Zhao, Y., Li, Y., Chang, L., Wang, Y., and Lin, H. (2021a). Shear Behaviors of Clay-Infilled Joint with Different Water Contents: Experiment and Model. *Arab. J. Geosci.* 14 (17), 1724. doi:10.1007/s12517-021-08207-8

Zhao, Y., Liu, Q., Zhang, C., Liao, J., Lin, H., and Wang, Y. (2021b). Coupled Seepage-Damage Effect in Fractured Rock Masses: Model Development and a Case Study. *Int. J. Rock Mech. Min. Sci.* 144, 104822. doi:10.1016/j.ijrmms.2021.104822

Zhao, Y., Wang, Y., and Tang, L. (2019). The Compressive-Shear Fracture Strength of Rock Containing Water Based on Druker-Prager Failure Criterion. *Arab. J. Geosci.* 12 (15), 452. doi:10.1007/s12517-019-4628-1

Zhao, Y., Wang, Y., Wang, W., Wan, W., and Tang, J. (2017a). Modeling of Non-linear Rheological Behavior of Hard Rock Using Triaxial Rheological Experiment. *Int. J. Rock Mech. Min. Sci.* 93, 66–75. doi:10.1016/j.ijrmms.2017.01.004

Zhao, Y., Zhang, C., Wang, Y., and Lin, H. (2021c). Shear-related Roughness Classification and Strength Model of Natural Rock Joint Based on Fuzzy Comprehensive Evaluation. *Int. J. Rock Mech. Min. Sci.* 137, 104550. doi:10.1016/j.ijrmms.2020.104550

Zhao, Y., Zhang, L., Wang, W., Pu, C., Wan, W., and Tang, J. (2016). Cracking and Stress-Strain Behavior of Rock-like Material Containing Two Flaws under Uniaxial Compression. *Rock Mech. Rock Eng.* 49 (7), 2665–2687. doi:10.1007/s00603-016-0932-1

Zhao, Y., Zhang, L., Wang, W., Wan, W., Li, S., Ma, W., et al. (2017b). Creep Behavior of Intact and Cracked Limestone under Multi-Level Loading and Unloading Cycles. *Rock Mech. Rock Eng.* 50 (6), 1409–1424. doi:10.1007/s00603-017-1187-1

Zhou, X.-P., Li, G.-Q., and Ma, H.-C. (2020). Real-time Experiment Investigations on the Coupled Thermomechanical and Cracking Behaviors in Granite Containing Three Pre-existing Fissures. *Eng. Fract. Mech.* 224, 106797. doi:10.1016/j.engfracmech.2019.106797

Zhou, X.-P., Zhang, J.-Z., Qian, Q.-H., and Niu, Y. (2019). Experimental Investigation of Progressive Cracking Processes in Granite under Uniaxial Loading Using Digital Imaging and AE Techniques. *J. Struct. Geol.* 126, 129–145. doi:10.1016/j.jsg.2019.06.003

Conflict of Interest: The authors declare that the research was conducted in the absence of any commercial or financial relationships that could be construed as a potential conflict of interest.

Publisher's Note: All claims expressed in this article are solely those of the authors and do not necessarily represent those of their affiliated organizations, or those of the publisher, the editors, and the reviewers. Any product that may be evaluated in this article, or claim that may be made by its manufacturer, is not guaranteed or endorsed by the publisher.